REVIEW OF FIXED TARGET EXPERIMENTAL RESULTS ON THE STRUCTURE OF THE PROTON*

BARBARA BADEŁEK

Physics Institute, University of Uppsala, S-751 21 Uppsala, Sweden
and
Institute of Experimental Physics, Warsaw University
Hoża 69, 00-681, Warsaw, Poland

(Received March 25, 1996)

At the end of the fixed-target deep inelastic scattering experimenal programme we summarize the developments on the structure of the proton that were studied in these experiments. We survey the latest structure function data and their QCD interpretation. Special attention is paid to the measurements taken in the low Q^2 region. The spin properties of the proton are discussed.

PACS numbers: 12.38.Qk

1. Introduction

In this article we review the status of the data on structure functions and derived quantities, obtained in the fixed-target, inelastic lepton scattering experiments. Until a few years ago this knowledge came entirely from fixed-target experiments. Now it is being complemented and extended by the results from the HERA *ep* collider, especially in the region of low x where the dynamics of a large number of confined partons has to be understood, as well as at very high scales where the perturbative assumptions can be further tested.

The (unpolarised) fixed-target deep-inelastic scattering programme will come to an end in 1996 except for the continuation of the CCFR neutrino experiments. Many experiments (SLAC, BCDMS, EMC, NMC, E665, CDHSW, BEBC and CCFR) have contributed to the heroic and successful

* Presented at the Cracow Epiphany Conference on Proton Structure, Kraków, Poland, January 5–6, 1996.

effort to obtain a fundamental and precise knowledge of properties of partons and of QCD. Characteristics of a number of them are listed in Table 1.1.

TABLE 1.1.

Fixed-target experiments contributing to the F_2 measurements. The x and Q^2 ranges refer to the F_2 data; structure function ratio measurements extend the low limits by approximately an order of magnitude.

Beam	Targets	Experiment	Q^2(GeV^2)	x
e	p,d,A	SLAC	0.6 – 30	0.07 – 0.8
μ	p,d,A	BCDMS	7.5 – 230	0.07 – 0.6
μ	p,d,A	NMC	0.5 – 75	0.006 – 0.6
μ	p,d,A	E665	0.2 – 75	0.0008 – 0.6
$\nu,\bar{\nu}$	Fe	CCFR, CDHSW	1.0 – 500	0.015 – 0.6

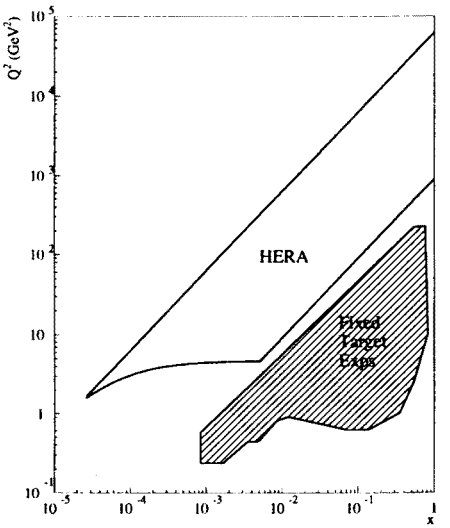

Fig. 1.1. The kinematical region covered by the HERA and fixed-target experiments (from [1]).

The kinematic plane covered by the fixed-target measurements and by HERA is shown in Fig. 1.1. Measurements at HERA can reach Q^2 (x) values two orders of magnitude larger (smaller) than those reached by fixed-target experiments but the two regions make contact and thus the continuity and normalization of the data can be checked. New upgrades of the HERA detectors will allow the exploration of even lower Q^2 in the future.

The fixed-target electron (muon) scattering experiments were almost always inclusive, *i.e.*information on the kinematic variables came only from measurements of the incident and scattered leptons. In the charged-current neutrino experiments the outgoing muon and the total energy of the produced hadrons are measured, and in neutral-current experiments only the latter is detected.

Charged lepton deep inelastic scattering (DIS) experiments benefit from high rates and low (unfortunately complicated) systematic biases. They however have to deal with a strong Q^2 dependence of the cross section (photon propagator effects) and with large contribution of radiative processes. Electron and muon measurements are complementary: the former offers very high beam intensities and thus statistics but its kinematic acceptance is limited to low values of Q^2 and moderate values of x, the latter extends to higher Q^2 and down to low values of x (an important aspect in the study of sum rules) but due to limited muon intensities the data taking time has to be long to ensure a satisfactory statistics. Neutrino deep inelastic experiments, able to separate quark and antiquark contributions (due to the V-A structure of the charged current weak interactions) suffer from low event rates and large systematic errors but offer an almost Q^2-independent and acceptance-undistorted cross section, only little contaminated by radiative events.

In deep-inelastic experiments the low x region is correlated with low values of Q^2, as shown in Fig. 1.1. For fixed-targets the lowest values of x were reached by the NMC at CERN and E665 Collaboration at FNAL applying special experimental techniques permitting measurements of muon scattering angles as low as 1 mrad. These "small x triggers" and special off-line selection methods were also effective against the background of muons scattered elastically from target atomic electrons which produce a peak at x =0.000545. Systematic errors on F_2 in both experiments (in particular those on the ratio of structure functions for different nuclei, F_2^a/F_2^b) were greatly reduced as a result of exposing several target materials at the time and/or by a frequent exchange of targets in the beam.

In the one-photon-exchange approximation, the differential electroproduction cross section is related to the structure function $F_2(x,Q^2)$ and the ratio $R(x,Q^2)$ of the cross sections for the longitudinally and transversally polarised virtual photons by

$$\frac{d^2\sigma(x,Q^2)}{dQ^2dx} = \frac{4\pi\alpha^2}{Q^4x}\left[1-y-\frac{Mxy}{2E}+\left(1-\frac{2m^2}{Q^2}\right)\frac{y^2(1+4M^2x^2/Q^2)}{2(1+R)}\right]F_2(x,Q^2)\,, \tag{1.1}$$

where M and m are the mass of the proton and the electron (muon) respectively, E and ν are the incident lepton energy and the energy transfer in the target rest frame, $y = \nu/E$, $x = Q^2/(2M\nu)$ and α is the electromagnetic coupling constant. The function $R(x, Q^2)$ has so far been measured only in fixed-target experiments, but even here information is scarce. The usual procedure to determine the $F_2(x, Q^2)$ is to assume a value of $R(x, Q^2)$ (theoretical, experimental or a combination of these) and then to extract $F_2(x, Q^2)$ from the data, using an iterative comparison of the experimental yield (corrected for acceptance, inefficiency of the apparatus as well as for higher-order QED processes) with the electroproduction cross section. At small x and Q^2 the assumed R values can be as large as 1. Note that a 20% error on R corresponds to about a 2% uncertainty on F_2 at $y = 0.6$ for R of about 0.6.

Section 2 of this article contains an overview of the data on (nucleon and nuclear) structure functions, of parton distribution measurements and of the sum rules. Our knowledge of the low Q^2 behaviour of F_2 is reviewed in Section 3. In Section 4 the spin structure of the proton is discussed and finally section 5 contains some brief conclusions. This article should be read together with that of A. De Roeck in these proceedings where the HERA results, complementing those discussed here, are presented.

2. Overview of structure function data

2.1. Structure function data

The NMC recently has presented their analysis of the proton and deuteron structure functions [2], in the range $0.006 \leq x \leq 0.6$ and $0.5 \leq Q^2 \leq 75$ GeV^2, as shown for F_2^d in Fig. 2.1, performed on the almost full sample of events. A clear scaling violation pattern with slopes $d \ln F_2 / d \ln Q^2$ positive at low x and an "approach to scaling" (*i.e.*a rise of F_2 from $Q^2 = 0$ to the scaling region) is visible. In this figure a comparison of the NMC, SLAC [3] and BCDMS [4] measurements is also shown. All three data sets are in good agreement with each other. They were thus used to obtain parametrizations of F_2^p and F_2^d and their uncertainties, using a 15–parameter function. The low x results of the EMC NA2 experiment have earlier been disproved by the NMC measurements. The data confirm a characteristic weak x dependence of F_2 at low Q^2, observed for the first time by the EMC NA28 experiment [5] and also interpreted in [6] (see also Section 3).

New measurements of the proton and deuteron structure functions for $x > 0.0001$ have recently been presented by the E665 Collaboration and are shown in Fig. 2.2 [7]. The lowest Q^2 and x values in their data are 0.2 GeV^2,

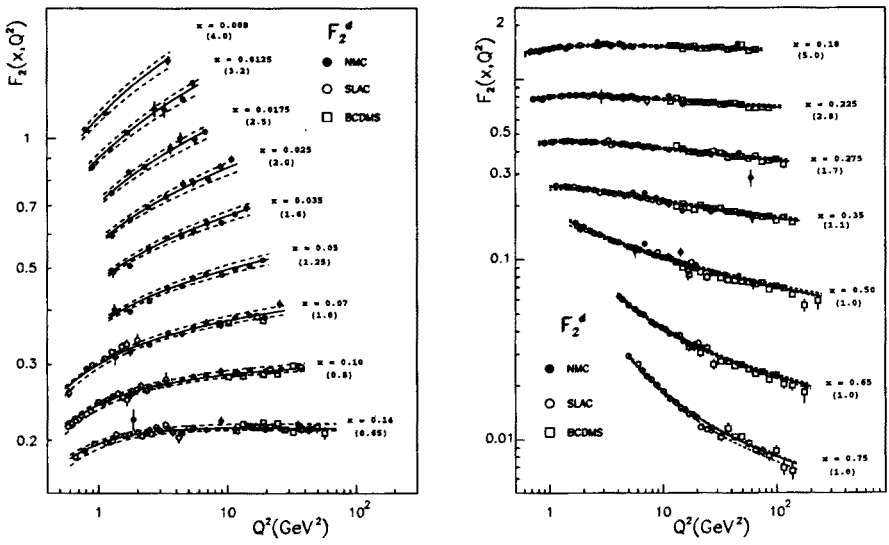

Fig. 2.1. The data from NMC compared with the data from SLAC and BCDMS. The errors are statistical. The solid curves are the results of a 15-parameter fit to all three data sets. The dashed curves correspond to the extreme values of the parameters (from [2]).

and 8×10^{-4}, respectively. A clear pattern emerges from these data at Q^2 values lower than a few GeV^2, namely a weak x, and possibly a stronger than logarithmic Q^2 dependence, of F_2.

The $x > 10^{-5}$ region is now being investigated by both the H1 and ZEUS Collaborations at HERA. The most dramatic effect visible in the HERA large Q^2 data is a strong increase of F_2 with decreasing x. This increase persists down to their lowest observed Q^2 ($Q^2 \approx 1.5$ GeV^2. At Q^2 values smaller than, say, 1 GeV^2 the x dependence of the F_2 is rather weak as observed by EMC NA28, NMC, and E665. It is probably due to the limited acceptance of the fixed-target data: for $Q^2 < 1.5$ GeV^2 these data are limited to moderate values of x. This can also be seen in Fig. 2.3 which shows for the high and moderate Q^2 data the strong rise of F_2 as a function of W, the invariant mass of the $\gamma^* p$ system (at low x, $W \simeq \sqrt{Q^2/x}$). F_2 is related to the total cross section of the proton-virtual photon interaction $\sigma_{tot}(\gamma^* p)$ via

$$\sigma_{tot}(\gamma^* p) \simeq \frac{4\pi^2\alpha}{Q^2} F_2(W, Q^2)\,. \tag{2.1}$$

The F_2 growth can be contrasted with the weak rise with W of the total real

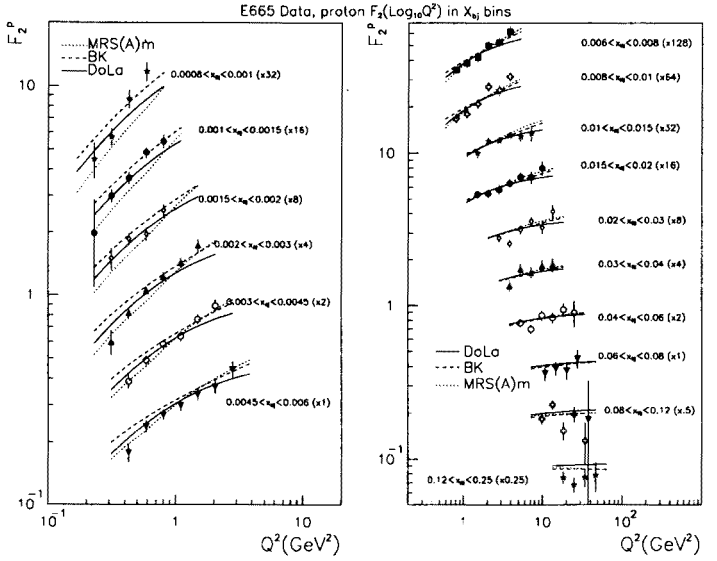

Fig. 2.2. Measurements of F_2^p by the E665 Collaboration. The errors are statistical and systematic added in quadrature, a normalisation uncertainty (1.8%) is not included. Curves show model calculations of Martin, Stirling and Roberts, Badełek and Kwieciński, and Donnachie and Landshoff (from [7]).

photoproduction cross section in the same range of W, as shown in Fig. 2.3. The different behaviour for $Q^2 = 0$ and data at a moderate Q^2 remains one of the interesting questions to be studied in the future.

The fixed-target F_2 data have had great impact on the determination of parton distributions (see *e.g.*[10]). It is now seen that these data join well to the results of HERA and thus make a joint QCD analysis possible in a large kinematic interval, [11]. In Fig. 2.4 a detailed comparison of the structure function F_2 as function of Q^2 between H1, ZEUS, E665 and NMC is shown for x values around 0.2, 0.07, 0.05 and 0.012. The data show a smooth continuation over the whole Q^2 region. It also shows a (still) substantially different level of accuracy between the HERA and the fixed-target experiments. The former are expected to improve both in statistics and systematics in the next few years. Apart from the above overall agreement, there exists however a discrepancy between the NMC and CCFR F_2 data at low x (not shown).

Both the NMC [12, 13] and E665 [14, 15] experiments have measured the deuteron-to-proton structure function ratio, F_2^d/F_2^p, extending down to

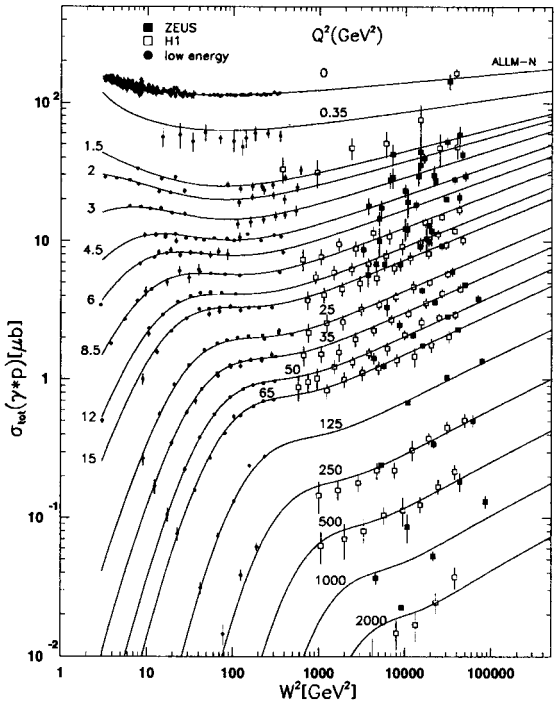

Fig. 2.3. Measurement of the proton structure function $F_2(W, Q^2)$ as function of W^2. The inner error bar is the statistical error. The full error represents the statistical and systematic errors added in quadrature. Also data at $Q^2 = 0$ are shown. Note that this figure contains the preliminary H1 data [8]. Curves are fits described in [9]. Figure taken from [1].

very low values of x. In the case of NMC the ratio has been measured directly, *i.e.*the measurement of the absolute structure function is used only for calculation of the radiative corrections. The data are usually presented as the ratio F_2^n/F_2^p where F_2^n is defined as $2F_2^d - F_2^p$. This quantity would give the structure function of the free nucleon in the absence of nuclear effects in the deuteron. The results are presented on the left in Fig. 2.5. In both data sets the average Q^2 varies from bin to bin reaching down to $\langle Q^2 \rangle = 0.2$ GeV^2 at x =0.0008 for the NMC and $\langle Q^2 \rangle = 0.004$ GeV^2 at $x = 5{\times}10^{-6}$ for E665. The results of both experiments show that the ratio F_2^n/F_2^p remains below unity down to the smallest measured values of x. At low x this can be attributed to nuclear shadowing in the deuteron [16], predicted to be only weakly x dependent, as observed. It seems unlikely that the results can also indicate a difference in F_2 of protons and neutrons

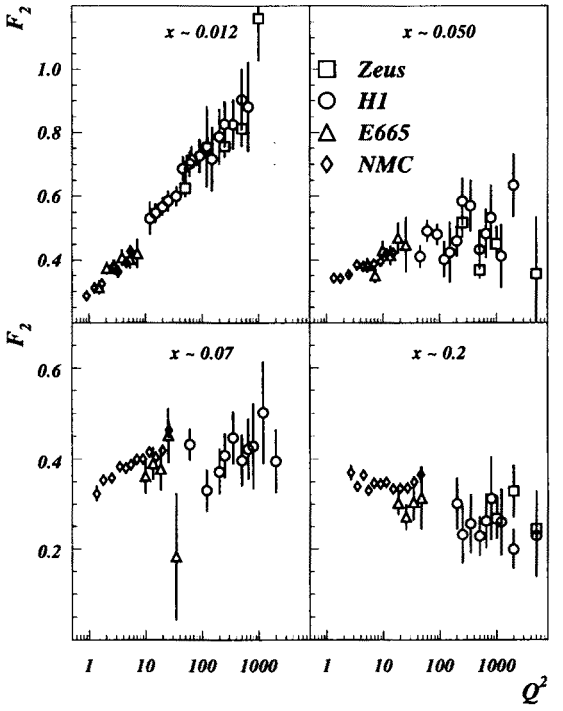

Fig. 2.4. Detailed comparison of the structure function F_2 as function of Q^2 between H1, ZEUS, E665 and NMC, for x values around 0.2, 0.07, 0.05 and 0.012. The error bars represent the full errors on the data points. Figure taken from [1].

at low x, since *e.g.*in Regge models the difference between the proton and neutron structure functions vanishes with decreasing x [16–18].

New data have appeared on nuclear shadowing. NMC have performed a high precision study of the A dependence of nuclear shadowing in the range $0.004 < x < 0.6$ and $1.5\ \mathrm{GeV}^2 < Q^2 < 60\ \mathrm{GeV}^2$. The results are shown on the right in Fig. 2.5 [19]. These measurements of the ratios F_2^A/F_2^C for A = Be, Al, Ca, Fe, Sn and Pb taken in conjunction with those on D, He, Li, C and Ca [20, 21] and with earlier data of SLAC [22], show a detailed pattern of the x dependence of shadowing. The NMC data range from $A = 2$ to $A = 208$. The functional dependence of F_2^A/F_2^C on A has been parametrized as $F_2^A/F_2^C = cA^{(\alpha-1)}$ in each bin of x. The amount of shadowing increases strongly with the mass number A. Lower values of x and Q^2 are covered by the nuclear data of E665 in the region x >0.0001 and Q^2 >0.1 GeV^2 [23], as shown in Fig. 2.6 (left). A decrease in the amount of shadowing observed by E665 is presently under discussion. Shadowing seems to saturate at x about 0.004 as also indicated by the NMC data on

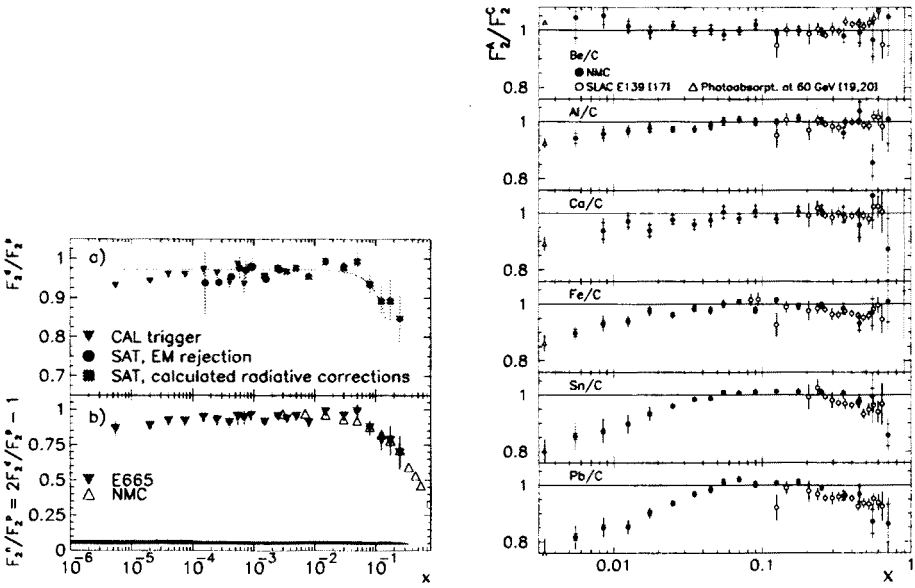

Fig. 2.5. **Left:** E665 results. a) — F_2^d/F_2^p for three different techniques of extracting the ratio. The curve shows a prediction of Badełek and Kwieciński, [16]. b) — $2F_2^n/F_2^p = 2F_2^d/F_2^p - 1$ as a function of x. The NMC data at Q^2 =4 GeV^2 are also shown. Errors are statistical. The systematic uncertainty is represented by the hatched area in Fig. b) (from [15]). **Right:** NMC results on F_2^A/F_2^C, averaged over Q^2 (open symbols) together with earlier results of SLAC (closed symbols). Inner/outer error bars represent the statistical/total errors. The SLAC-E139 data for silver and gold were used for the comparison with the tin and lead data of the NMC, respectively. The photoproduction cross section data are given at a small value of x for convenience (from [19]).

the F_2^{Li}/F_2^D and F_2^C/F_2^D ratios measured down to x =0.0001 and Q^2=0.03 GeV^2 [21]. No clear Q^2 dependence is visible in the E665 data in a wide interval of Q^2, shown in Fig. 2.6 (right), contrary to the preliminary NMC results in which positive Q^2 slopes for the F_2^{Sn}/F_2^C ratio at $x < 0.1$ are observed, as shown in [24]. The shadowing region seems to have another interesting feature: it contains a large fraction of large rapidity gap (or diffractive) events, their fraction increasing with A [25].

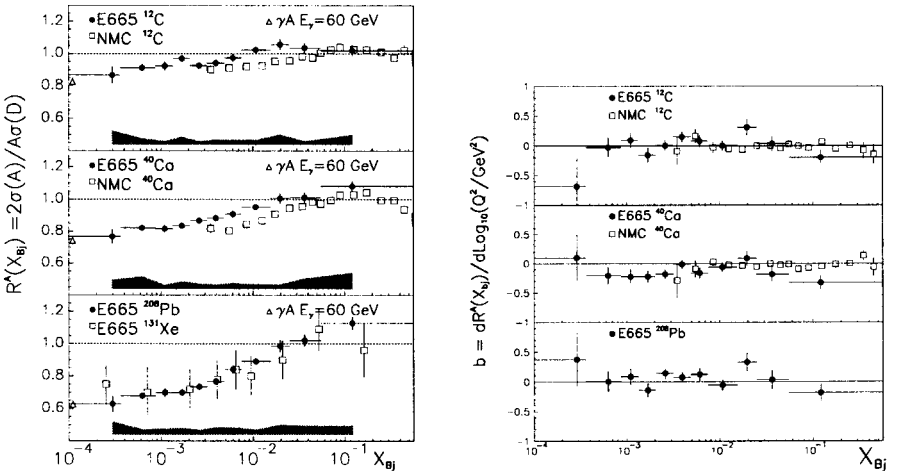

Fig. 2.6. **Left:** E665 results on σ^A/σ^D. Errors are statistical, the systematic ones are marked as shaded bands. Overall normalisation uncertainties have not been included. The NMC results have been shown for comparison where available (from [23]). **Right:** Q^2 dependence of the E665 F_2^A/F_2^D data (closed circles). Errors result from the fit, in which only statistical errors were considered. The NMC results are drawn as open squares (from [23].

2.2. Parton distribution measurements

NLO QCD fits have been performed by the NMC to their (earlier) accurate measurements of the structure functions F_2^p and F_2^d down to low values of x [26]. The flavour singlet and non-singlet quark distributions as well as the gluon distribution have been parametrized at the reference scale equal to 7 GeV^2. All the data with $Q^2 \geq 1$ GeV^2 were included in the fit. Besides the leading twist contribution a higher twist term was also included using a factor $1 + H(x)/Q^2$ where $H(x)$ was determined from the SLAC and the BCDMS measurements [27], averaged over the proton and deuteron, and suitably extrapolated to lower values of x. Results of the QCD fit to the proton structure function data are shown in Fig 2.7 and clearly indicate the extension of the QCD analysis to the low x and low Q^2 regions. The contribution of higher twists is however substantial at scales of about 1 GeV^2. Results of the NLO QCD fits performed by HERA do not support this conclusion, [11], but they may need to be reviewed when higher precision data at low x become available.

Additional information on the gluon density is extracted from hadronic final states. The E665 experiment has used the energy–energy angular pat-

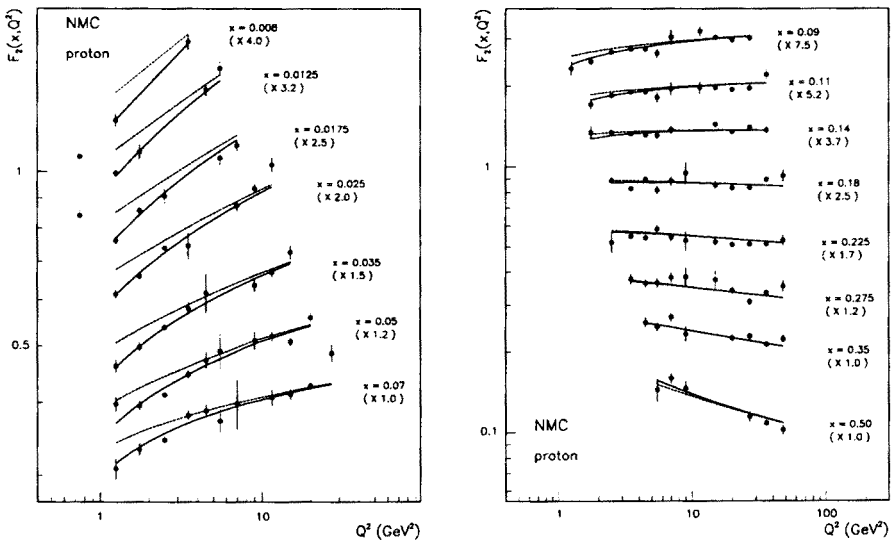

Fig. 2.7. The results of the QCD fit to the F_2^p data. The solid line is the result of the QCD fit with higher twist included. The dotted curve shows the contribution of the leading twist F_2. The errors are statistical (from [26]).

tern of hadrons produced in DIS to extract the gluon distribution function of the nucleon, down to x=0.005, [25]. Results agree with these of the H1 experiment where the gluon density was extracted from 2-jet events at $x \geq 0.001$, [11].

The presence of diffractive-like events in the DIS event sample (about 10% of the HERA sample) has so far been neglected in the QCD analyses. This problem should be considered in the future.

2.3. $R(x, Q^2)$ measurements

Extraction of $F_2(x, Q^2)$ from the data needs information on $R(x, Q^2)$. In particular the ratio of inelastic cross sections on different nuclei is only equal to the corresponding structure function ratio, provided $R(x, Q^2)$ is the same for these nuclei. Results of the NMC analysis on $R^{Ca} - R^C$ [28] and $R^d - R^p$ [29], shown in Fig 2.8 (left), demonstrate that neither of these quantities exhibit a significant dependence on x and that they are both compatible with zero. The NMC reported preliminary measurements of $R(x, Q^2)$ for proton and deuteron targets as a function of x in the range $0.006 < x < 0.14$ [30]. The average Q^2 of these measurements ranges from 1.1 GeV^2 at the smallest x to 15.5 GeV^2 at x =0.14. The results show a

rise of R with decreasing (small) x. Preliminary measurements of $R(x, Q^2)$ on a heavy target (Fe), at $x > 0.01$ and $Q^2 > 4$ GeV^2 (at present) have also been reported by the CCFR neutrino Collaboration [31].

In their data analyses the NMC and E665 experiments assumed R was independent of the target atomic mass A and given by the SLAC parametrization [32] valid for $x > 0.1$ and $Q^2 > 0.3$ GeV^2. This parametrization was then extrapolated (assuming 100% error) to $Q^2 \to 0$. Hence there is a need of a theoretical estimate of R (or F_L) in the region of low x and low Q^2. Two new phenomenological studies make an attempt to deliver such estimates. In these studies both the perturbative QCD contribution, which at low x and low Q^2 is dominated by the photon-gluon mechanism, and a non-perturbative term are taken into account. In [33] the latter contribution is determined phenomenologically (Fig. 2.8 (right)) while in [31] it is fitted to the low Q^2 data.

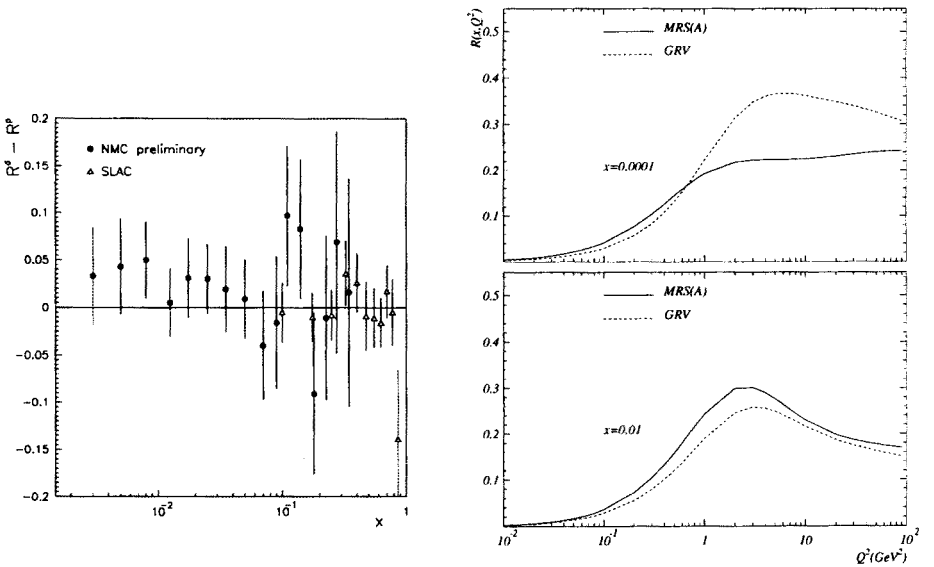

Fig. 2.8. **Left:** NMC (preliminary) results $R^d - R^p$ compared with the QCD predictions (the curve) and with the results of SLAC (open symbols), from [29]. **Right:** $R(x, Q^2)$ in the phenomenological model of Badełek, Kwieciński and Stasto, for two different parton parametrisations (from [33]).

Also at HERA the study of R is an issue of interest. For this purpose it has been proposed to operate HERA at lower energies, to have the cross section measurements at two y values for a given x, Q^2 point. Such a measurement could be done in 1996 or 1997.

2.4. Sum rules

Several sum rules have been formulated for different combinations of structure functions. Strict QCD predictions, valid for $Q^2 \to \infty$, exist for those involving only flavour nonsinglet contributions: the Gross–Llewellyn-Smith and the Bjorken sum rules. Experimental measurements of such sum rules provide a stringent test of fundamental QCD assumptions. They also in principle permit the extraction of the strong coupling constant, α_S, from the data. Due to the finite Q^2 of the measurements, a predicted value of a sum rule is usually presented in the form of a power series in α_S, the coefficients of which are directly calculated.

There is no strict QCD prediction for the sum rules containing the flavour singlet contributions, *i.e.*the Gottfried and Ellis–Jaffe sum rules. The reason is that singlet contributions contain an "intrinsic" Q^2 dependence due to the anomalous dimension of the singlet axial vector current. Testing them usually results in surprises which teach us a lot about the shortcomings of the simple quark model.

All the sum rules involve integrations over the whole $0 \leq x \leq 1$ interval. This means that due to the limited experimental acceptance, interpolations from x_{min} to 0 and from x_{max} to 1 have to be performed. Usually the former is more problematic due to a larger contribution of the small x region to integrals and/or to a poor theoretical understanding of this kinematic region. Thus the extrapolation $x \to 0$ is a major source of systematic errors in such sum rule tests. Another source is produced by the limited experimental acceptance in Q^2 at each x value. This usually means that a sum rule is measured at a certain Q_0^2, common to all points but at values of Q_0^2 which are not sufficiently high to exclude a contribution from nonperturbative effects ("higher twists").

2.4.1. Tests of the flavour nonsinglet sum rules.

The Bjorken sum rule involves the spin structure functions and will be presented in Section 4. The Gross-Llewellyn-Smith sum rule, formulated within the Quark Parton Model, states that the integral over the valence quark densities is equal to 3 *i.e.*$\int_0^1 xF_3(x)dx/x=3$. The QCD corrections to this rule have been calculated up to α_S^3 [34]. The sum rule has been tested by the CCFR Collaboration in conjunction with additional low energy data from bubble chamber experiments [35]. The sum rule is fulfilled at the 10% accuracy level. The value of α_S has been obtained at Q^2=3 GeV^2; it corresponds to $\alpha_S(M_Z) = 0.108^{+0.003}_{-0.005}(\text{stat.}) \pm 0.004(\text{syst.})^{+0.004}_{-0.006}(\text{HT})$. The uncertainty due to the low scale of the measurement (*i.e.*the presence of "higher twists") dominates the statistical error.

2.4.2. Tests of the flavour singlet sum rules.

The NMC measurements of F_2^d (fitted together with the SLAC and BCDMS data) and of F_2^n/F_2^p allow a determination of the Gottfried sum *i.e.*$S_G = \int (F_2^p - F_2^n)dx/x$ where $F_2^p - F_2^n = 2F_2^d(1 - F_2^n/F_2^p)/(1 + F_2^n/F_2^p)$. At Q^2 =4 GeV^2, neglecting any Q^2 dependence, S_G was found to be 0.235 $\pm$ 0.026 [13], significantly below the simple quark–parton model value of 1/3. This is evidence for a flavour asymmetric sea in the nucleon ($\bar{d}$ sea quarks carry more momentum than $\bar{u}$), a fact confirmed by the NA51 measurement of the Drell-Yan asymmetry in pp and pn collisions, which gave: $\bar{u}/\bar{d}$=0.51$\pm$0.04$\pm$0.05 at x=0.18 and Q^2=25 GeV^2 [36]. Recently a non-negligible Q^2 dependence of $F_2^p - F_2^n$ as a function of x at low Q^2 has been reported by the NMC: both the position of the maximum and the maximum value of this function change with Q^2. This change becomes negligible when higher twist contributions are separated out from the F_2^d and F_2^n/F_2^p measurements [37]. The Ellis–Jaffe sum rule, involving the spin structure functions will be discussed in Section 4.

3. Low Q^2, low x insights from fixed-target data

3.1. Introduction and basic concepts

Due to the experimental constraints the fixed-target studies of deep inelastic scattering at low x necessarily were correlated with low Q^2 ($Q^2 \lesssim 1$ GeV^2). There are two reasons why this kinematic region is of special interest. First, as emphasized in Section 2, the fixed-target and HERA measurements at small x highlight the importance of a theoretical understanding of the connection between the low Q^2 and high Q^2 behaviour. The second is a practical reason; a unified treatment of low and high Q^2 is essential for the large Q^2 deep inelastic scattering data analysis, since to implement radiative corrections we require a knowledge of structure functions for $Q^2_{\rm meas} \geq Q^2 \geq 0$.

At low Q^2 there are constraints on the structure functions $F_i(x, Q^2)$ which follow from eliminating the kinematical singularities at $Q^2 = 0$ from the hadronic tensor $W^{\mu\nu}$. It is easy to show that as $Q^2 \to 0$ we require

$$F_2 = O(Q^2) \quad \text{and} \quad F_L = O(Q^4)\,. \tag{3.1}$$

Hence it is clear that Bjorken scaling, which holds approximately at high Q^2, cannot be a valid concept at low Q^2.

In dealing with low Q^2 data we need to introduce the concept of "higher twists". The operator product expansion leads to the representation

$$F_2(x, Q^2) = \sum_{n=0}^{\infty} \frac{C_n(x, Q^2)}{(Q^2)^n}\,, \tag{3.2}$$

where the functions $C_n(x,Q^2)$ depend weakly (*i.e.*logarithmically) on Q^2. The various terms in this expansion are referred to as leading ($n=0$) and higher ($n \geq 1$) twists. The QCD improved parton model where

$$F_2(x,Q^2) \;=\; x\sum_i e_i^2\,[q_i(x,Q^2)+\overline{q}_i(x,Q^2)] \;+\; O(\alpha_S(Q^2))\,, \qquad (3.3)$$

and which gives approximate Bjorken scaling, retains only the leading twist contribution. Physically the higher twist effects arise from the struck parton's interaction with target remnants, thus reflecting confinement. For Q^2 of the order of a few GeV^2, contributions of the "higher twists" may become significant, see, for example, Ref. [26]. Contrary to the common opinion higher twists, which are corrections to the leading (approximately scaling) term (3.3), can only be implemented for sufficiently large Q^2. Thus they cannot correctly describe the low Q^2 (*i.e.*nonperturbative) region since the expansion (3.2) gives a divergent series there. In particular the individual terms in this expansion violate the constraint (3.1). In order to correctly describe this region the (formal) expansion (3.2) has to be summed beforehand, at large Q^2, and then analytically continued to the region of $Q^2 \sim 0$. This is automatically embodied in certain models like the Vector Meson Dominance (VMD) model. To be precise the VMD model together with its generalisation which gives (approximate) scaling at large Q^2 can be represented in a form (3.2) for sufficiently large Q^2.

In practical applications to the analysis of experimental data which extend to the moderate values of Q^2 one often includes the higher twists corrections in the following simplified way:

$$F_2(x,Q^2) = F_2^{LT}(x,Q^2)\left[1+\frac{H(x)}{Q^2}\right], \qquad (3.4)$$

where the F_2^{LT} is the leading twist contribution to F_2 and $H(x)$ is determined from fit to the data. This simple minded expression may not be justified theoretically since in principle the higher twist terms, *i.e.*functions $C_n(x,Q^2)$ for $n \geq 1$ in Eq. (3.2) evolve differently with Q^2 than the leading twist term.

Here we give a brief overview of the parametrizations and the data in the low x, low Q^2 region. We refer the reader to Refs. [38] and [39] for a more detailed review of the treatment of low Q^2 problems.

3.2. Parametrisations of structure functions

There exist several phenomenological parametrisations (fits) of the structure function F_2 which incorporate the $Q^2 \to 0$ constraints as well as the

Bjorken scaling behaviour at large Q^2 [40–45]. Certain parametrisations [43–45] also contain the (QCD motivated) scaling violations. However, they usually are not linked with the conventional QCD evolution. Nor is the low Q^2 behaviour related to the explicit vector meson dominance, known to dominate at low Q^2. There exist parmetrisations which explicitly contain QCD evolution: [46, 6, 47, 48]. Most of the parametrisations essentially extend the parton model formula for F_2 down to the low Q^2 region modifying in a suitable way the parton distributions; the model [6] includes also the VMD contribution besides the partonic one and is an absolute prediction (*i.e.*no fitting to the data). The low Q^2 modifications are typically the following ones:

(i) Instead of the variable x, modified variables $\bar{x}_i = x(1 + Q_{0i}^2/Q^2)$ are used as arguments of the parton distributions where 'i' enumerates the type of the parton.

(ii) Models which at large Q^2 include the QCD scaling violations, have the evolution in Q^2 either "frozen" below certain scale $\bar{Q}_0^2$ which is of the order of 1 GeV^2 or the evolution in a "shifted" variable $Q^2 + \bar{Q}_0^2$ is used.

(iii) Parton distribution functions are multiplied by form factors of the type $Q^2/(Q^2 + m_i^2)$ which ensure vanishing of the structure function $F_2(x, Q^2)$ at $Q^2 = 0$.

Modifications are absent in the dynamical model [46] which, in principle, is meant to describe the structure functions only in the large Q^2 region even if the QCD evolution is extended down to very low scales. Also the recent parametrisation of the "parton distributions" [48] uses the variable x instead of $\bar{x}$. This model does not however extend down to the very low values of Q^2 (*i.e.*for $Q^2 < 0.25$ GeV^2) and, in particular, it does not accommodate the photoproduction.

Parametrisations of $F_2(x, Q^2)$ differ in their small x behaviour. Most of them (except [44] and [42]) incorporate at large Q^2 the steep rise of $F_2(x, Q^2)$ as the function of x with decreasing x which is much stronger than implied (for instance) by the expectations based on the "soft" pomeron with intercept $\alpha_P = 1.08$. This steep increase of $F_2(x, Q^2)$ becomes very weak at low Q^2. Possible dynamical origin of this effect is different in different models being either attributed to the absorptive effects [45, 47, 48], to the onset of the VMD mechanism [6] or to the pure perturbative QCD effects related to the change of the "evolution length" [46].

There exists practically only one parametrisation of the $R(x, Q^2)$ structure function for the nucleon, *i.e.*the SLAC parametrisation, [32], based on measurements by SLAC, EMC, BCDMS and CDHSW and valid at $x > 0.1$ and $Q^2 > 0.3$ GeV^2. Experimental analyses in DIS experiments need to

know R down to measured values of x and for $0 < Q^2 < Q^2_{\text{meas}}$. Two phenomenological studies deliver estimates of R in the unmeasured region. Both the perturbative QCD contribution, which at low x and low Q^2 is dominated by the photon-gluon mechanism, and a non-perturbative term are there taken into account. In [33] the latter contribution is determined phenomenologically while in [31] it is fitted to the low Q^2 data.

3.3. Experimental data

The lowest values of x, correlated with lowest values of Q^2 ($x \sim 10^{-5}$ and $Q^2 \sim 0.001$ GeV^2), were reached by the E665 Collaboration at Fermilab by applying a special experimental technique which permits the measurement of muon scattering angles as low as 1 mrad. At HERA the lowest values of Q^2 (1.5 GeV^2) were recently reached by two methods: shifting the interaction point in the proton beam direction in order to increase the acceptance of low Q^2 events and by using radiative events with hard photon emission collinear with the incident electron, [11]. The radiative events can be interpreted as non-radiative ones with reduced electron beam energy.

During the last three years an abundance of new data reaching Q^2 values smaller than 1 GeV^2 have appeared. These comprise: results on the proton and deuteron structure functions from NMC ($x > 0.006, Q^2 > 0.5$ GeV^2) [2, 49] Fig. 2.1, and E665 ($x > 0.0001, Q^2 > 0.2$ GeV^2) [7] Fig. 2.2, results on the deuteron-to-proton structure function ratio, F_2^d/F_2^p, measured by NMC and E665 for $x > 0.0008$, $Q^2 > 0.2$ GeV^2 (NMC [13, 12]) and $x > 0.000\,005$, $Q^2 > 0.004$ GeV^2 (E665 [14, 15], Fig. 2.5 (left), precise results from these two collaborations on x, A and Q^2 dependence of nuclear shadowing [19, 21, 24, 20, 50, 23], Fig. 2.5 (right) and Fig. 2.6; and measurements of $R^{Ca} - R^C$ [28], $R^d - R^p$ [29], Fig. 2.8 (left), R^p and R^d at low x by NMC [30] and R^A at low x by CCFR [31].

The above-mentioned data were presented and discussed in Section 2. Here we shall add only a few remarks connected with their low Q^2 behaviour. The data on the nucleon F_2 display a weak x, and possibly a stronger than logarithmic Q^2, dependence, at Q^2 lower than a few GeV^2. Observe that also the photoproduction cross section between the fixed-target and HERA energies increases rather weakly with energy, *cf.* Fig. 2.3. This should be contrasted with measurements at HERA for Q^2 larger than a few GeV^2, which show a strong increase of F_2 with decreasing x, [11]. The QCD analysis of the NMC F_2 data, [26], shows that the contribution of higher twists of the form similar to (3.4) is moderate even at scales about 1 GeV^2, Fig. 2.7. This is visible in Fig. 2.2, where the $F_2^p(x, Q^2)$ at low Q^2 is well described by models [6, 42] directly containing higher twist contributions. The higher twists seem also to account for the Q^2 dependence of the $F_2^p - F_2^n$ function, *cf.* Section 2.4.2.

The F_2^d/F_2^p ratio, Fig. 2.5 (left), which stays always below unity down to the smallest measured values of x, reflects nuclear shadowing in the deuteron, only weakly dependent on x. The data are well described by a model [16], which contains the VMD part, essential at low Q^2, and which relates shadowing to the diffractively produced final states. The agreement extends over nearly five orders of magnitude in x. No clear Q^2 dependence is visible in the shadowing data in a wide interval of Q^2, neither in F_2^d/F_2^p nor in F_2^A/F_2^D [15, 23], *cf.* Fig. 2.6 (right), except possibly for $F_2(Sn)/F_2(C)$ at $x < 0.1$, [24]. Shadowing thus appears as a leading twist phenomenon.

3.4. Outlook

In this section we have listed the ideas and results concerning the electroproduction structure functions in the region of low values of x and Q^2. $F_2(x, Q^2)$ should vanish linearly with Q^2 for $Q^2 \to 0$ (for fixed ν), an important property which follows from the conservation of the electromagnetic current. The purely partonic description of inelastic lepton scattering has thus to break down for low Q^2. At moderate Q^2 the higher twist contributions to F_2 which vanish as negative powers of Q^2 are sometimes included in the QCD data analysis. One also expects at low Q^2 that the VMD mechanism should play an important role.

The small x behaviour of $F_2(x, Q^2)$ is dominated by pomeron exchange. Analysis of the structure function in the small x region for both low and moderate values of Q^2 can clarify our understanding of the pomeron. At large Q^2 the problem is linked with the QCD expectations concerning deep inelastic scattering at small x [51]. Besides the structure functions (or total cross sections) complementary information on the pomeron can also be obtained from the analysis of diffractive processes in the electro- and photoproduction. This concerns both inclusive diffraction and diffractive production of vector mesons [9].

Descriptions of the low Q^2, low x behaviour of F_2 range from pure fits to experimental data to dynamically motivated models.

There now exists a wealth of measurements of F_2 in the low Q^2, low x region. These include the NMC and E665 results which extend down to very low x and Q^2 and display characteristic "approach to scaling" behaviour, as well as the first results from HERA at Q^2 which extend down to 1.5 GeV^2. The data were QCD analysed, showing its applicability down to scales of the order of 1 GeV^2. Nuclear shadowing was studied in great detail for targets ranging from $A = 2$ to $A = 208$ by the NMC and E665 collaborations. Its x, Q^2 and A dependence were precisely measured. Preliminary data on $R(x, Q^2)$ have also been reported (NMC and CCFR).

The fixed-target (unpolarised) structure function measurement programme comes to an end in 1996. Many experiments contributed in a

great and successful effort to learn about properties of partons and strong interactions. Several aspects of this knowledge are yet not understood. One of these and perhaps the most challenging one is low x dynamics and in particular its dependence on the probing photon virtuality, Q^2. The new possibilities concerning the study of this problem have opened up with the advent of HERA. The data collected there show a very strong increase of F_2 with decreasing x at high Q^2. This increase becomes weaker at low Q^2, an effect known for a long time from the fixed-target measurements. These data bridge the gap between the fixed-target and the collider low x results, thus opening a possibility of a unified understanding of the underlying dynamics.

4. Spin physics

Interest in spin phenomena in deep inelastic scattering revived in the eighties after the European Muon Collaboration discovered that the spin dependent structure function of the proton violates the Ellis-Jaffe sum rule and that the quarks probably carry only a small part of the total proton spin. The problem of the origin of the proton spin has led to an intense experimental and theoretical activity but in spite of that it has not yet been answered conclusively. Here we briefly review the status of the spin effects in deep inelastic scattering: experimental results, their interpretation and future prospects of the spin physics.

4.1. Cross section asymmetries and sum rules

The deep inelastic lepton-nucleon scattering cross section is the sum of a spin independent term $\overline{\sigma}$, *cf.* 1.1 and a term proportional to the lepton helicity h_l:

$$\sigma = \overline{\sigma} + \tfrac{1}{2} h_l \Delta\sigma \,. \tag{4.1}$$

Only longitudinally polarised leptons will be considered and the spin vector s_l is thus related to the lepton four momentum vector k. $\Delta\sigma$ gives only a small contribution to the total deep inelastic cross section. It depends on the two structure functions g_1 and g_2 and can be expressed as

$$\Delta\sigma = \cos\psi \, \Delta\sigma_{\parallel} + \sin\psi \cos\phi \, \Delta\sigma_{\perp} \,, \tag{4.2}$$

with

$$\begin{aligned} \frac{\mathrm{d}^2\Delta\sigma_{\parallel}}{\mathrm{d}x\mathrm{d}Q^2} &= \frac{16\pi\alpha^2 y}{Q^4}\left[(1-\frac{y}{2}-\frac{\gamma^2 y^2}{4})g_1 - \frac{\gamma^2 y}{2} g_2\right], \\ \frac{\mathrm{d}^3\Delta\sigma_T}{\mathrm{d}x\mathrm{d}Q^2\mathrm{d}\phi} &= -\cos\phi \, \frac{8\alpha^2 y}{Q^4}\gamma\sqrt{1-y-\frac{\gamma^2 y^2}{4}}\left(\frac{y}{2}g_1 + g_2\right). \end{aligned} \tag{4.3}$$

In the above expressions, ψ denotes the angle between the lepton and the nucleon spin and ϕ the angle between the scattering plane and the spin plane; furthermore $\Delta\sigma_\perp = \Delta\sigma_T/\cos\phi$ and $\gamma = 2Mx/\sqrt{Q^2}$ is a kinematical factor.

In experimental measurements, two asymmetries can be defined:

$$A_\parallel = \frac{\Delta\sigma_\parallel}{2\bar{\sigma}} \qquad \text{and} \qquad A_\perp = \frac{\Delta\sigma_\perp}{2\bar{\sigma}}. \tag{4.4}$$

These asymmetries are directly related to the virtual photon asymmetries, A_1 and A_2:

$$A_\parallel = D(A_1 + \eta A_2), \qquad A_\perp = D(A_2 - \xi A_1), \tag{4.5}$$

where

$$A_1 = \frac{g_1 - \gamma^2 g_2}{F_1}, \qquad A_2 = \gamma\frac{g_1 + g_2}{F_1}. \tag{4.6}$$

D, often called the depolarisation factor of the virtual photon, depends on y and the structure function $R = F_L/F_T$; factors η and ξ depend only on kinematic variables. A_1 and A_2 are often interpreted as virtual photon–nucleon asymmetries. They satisfy the bounds $|A_1| \leq 1$, $|A_2| \leq \sqrt{R}$.

Within the QPM the spin dependent structure function g_1 is given by

$$g_1(x) = \frac{1}{2}\sum_{i=1}^{n_f} e_i^2[\Delta q_i(x) + \Delta\bar{q}_i(x)], \tag{4.7}$$

with $\Delta q_i(x) = q_i^+(x) - q_i^-(x)$, where $q^\pm$ are the distribution functions of quarks with spin parallel (antiparallel) to the nucleon spin. Less obvious is the meaning of g_2 which contains a leading twist part, completely determined by g_1 and a higher twist part, the meaning of which is subject to debate [52]. In QCD, g_1 evolves according to Altarelli–Parisi equations, similar to the unpolarised ones. Corresponding coefficient and splitting functions have recently been calculated up to order α_S^2 [53], permitting the next-to-leading order QCD analysis of g_1 and thus a determination of the polarised parton distributions, $\Delta q_i(x, Q^2)$. Various groups have used the recent data to determine these distributions, taking into account the leading order QCD corrections.

A comparison of different parametrizations [54] shows that the polarised valence quark distributions $\Delta u_v(x, Q^2)$ and $\Delta d_v(x, Q^2)$ can be determined with some accuracy from the data, while the polarised sea quark and gluon distributions $\Delta\bar{q}(x, Q^2)$ and $\Delta g(x, Q^2)$ are only loosely constrained by the structure function measurements.

Contrary to g_1 and g_2, definite theoretical predictions exist for the first moment of g_1, $\Gamma_1 = \int_0^1 g_1(x)\,\mathrm{d}x$, which measures the expectation value of the axial vector current between two nucleon states. Two sum rules exist for Γ_1. The fundamental one was obtained by Bjorken [55] from the current algebra and isospin symmetry between the proton and the neutron:

$$\Gamma_1^{\mathrm{p}} - \Gamma_1^{\mathrm{n}} = \frac{1}{6}\left|\frac{g_A}{g_V}\right| = \frac{1}{6}(\Delta u - \Delta d)\,, \tag{4.8}$$

where g_A and g_V are the axial and vector weak coupling constants in the neutron beta decay. The QCD corrections to this sum rule have been computed up to the order α_S^3 [56] and the $\mathcal{O}(\alpha_S^4)$ have been estimated [57].

Separate sum rules, obtained by Ellis and Jaffe [58], hold for the proton and the neutron:

$$\Gamma_1^{p(n)} = \pm\frac{1}{12}\left|\frac{g_A}{g_V}\right| + \frac{1}{36}a_8 + \frac{1}{9}\Delta\Sigma\,. \tag{4.9}$$

Here $\Delta\Sigma = \Delta u + \Delta d + \Delta s$ is the flavour singlet axial coupling and Δq denote first moments of the spin dependent parton distributions in the proton, $\Delta q = \int_0^1 \Delta q_i(x)\,\mathrm{d}x$; a_8 (and $|g_A/g_V|$) are related to the symmetric and antisymmetric weak flavour-SU(3) couplings in the baryon octet. If the flavour-SU(3) is exact then a_8 can be predicted from measurements of hyperon dacays. There is however no prediction for $\Delta\Sigma$, except for Δs=0. In this case $\Delta\Sigma = a_8$, as was assumed in the original formulation by Ellis and Jaffe [58]. QCD corrections to these sum rules have been calculated up to the order α_S^2 [59] and the $\mathcal{O}(\alpha_S^3)$ have been estimated [60]. Due to the axial anomaly of the singlet axial vector current, $\Delta\Sigma$ is intrinsically Q^2–dependent. Depending on the factorization scheme applied [61] this results either in a scale–dependence of the sea quark polarization or in an extra contribution to the Ellis–Jaffe sum rule, involving $\Delta g = \int_0^1 [g^+(x) - g^-(x)]\,\mathrm{d}x$, the gluonic equivalent of the quark distribution moments. Both formulations are equivalent.

Higher twist effects in the Q^2 dependence of Γ_1 will not be considered here.

Evaluation of the Γ_1 requires knowledge of g_1 in the entire interval from 0 to 1. Measurements cover a limited kinematic range and thus extrapolations of g_1 to 0 and 1 are necessary. The latter is not critical since $g_1 \to 0$ at $x \to 1$ but the former is a considerable problem since g_1 increases as x decreases and its behaviour at low x is theoretically not understood. Therefore results on Γ_1 depend on the assumptions made in the $x \to 0$ extrapolation. Both SMC and SLAC experiments assume the Regge like behaviour of g_1,

*i.e.*that at $x \to 0$, g_1 behaves like x^α, $0 \leq \alpha \leq 0.5$. A value α=0 was chosen and g_1 was fitted to the two data points at lowest x, allowing for variation of this behaviour within the Regge model. This approach might however be inconsistent with QCD which predicts a faster rise of g_1 at low x.

4.2. Experiments

New generation polarised electroproduction experiments are listed in Table 4.1.

The experiment of the Spin Muon Collaboration (SMC) at CERN uses a naturally polarised muon beam and a cryogenic, solid state target. Experiments E142 – E155 at SLAC use an electron beam and liquid (solid) cryogenic targets. The HERMES experiment at DESY uses an electron beam from the HERA collider and internal gas targets. The scattered muon spectrometers in the SMC and SLAC experiments have been used (with little change) in DIS experiments preceeding the polarised programme, contrary to the HERMES apparatus.

TABLE 4.1.

New generation experiments on polarised deep inelastic charged lepton–nucleon scattering. The last column shows references to the principal physics results obtained until now, (from [62]).

Experiment	Beam	Year	Beam energy (GeV)	Target	References
SMC	μ^+	1992–5	100,190	C_4D_9OD	[63, 64]
		1993	190	C_4H_9OH	[65, 66]
		1996	190	NH_3	
E142	e^-	1992	19.4 –25.5	^3He	[67]
E143	e^-	1993	29.1	NH_3, ND_3	[68, 69]
E154	e^-	1995	50	^3He	
E155	e^-	1996	50	NH_3, ND_3	
HERMES	e^-	1995–	30–35	H, D, ^3He	

The lowest x in the results published by the SMC is about 10^{-3} and corresponds to Q^2 about 1 GeV^2. In the course of analysis are events having lower Q^2 and reaching x values of 10^{-4}. A special trigger has been set up recently to extend the measurements down to x=10^{-5}, at the expense of lowering Q^2 to 0.01 GeV^2. The upper limit of Q^2 in the SMC is about 100 GeV^2. The SLAC experiments' acceptance extends from x about 0.01 at $Q^2 = 1$ GeV^2 up $Q^2 \approx 10$ GeV^2 at $x \sim 0.7$. As in all fixed-target experiments, the low values of x in the SMC and SLAC are correlated with low Q^2.

The cross section asymmetry measured in the polarised lepton — polarised nucleon experiments, $A_{\rm exp}$, is related to the asymmetries defined

in Eq. (4.4) by $A_{\rm exp} = fP_tP_bA$ where P_t, P_b denote the target and beam polarisations and f, the target dilution factor, accounts for the fact that only a fraction of nucleons is polarised. The beam polarisation at the SMC has been measured with a purpose-built polarimeter, using two independent methods: polarised μe scattering and an analysis of the energy spectrum of electrons coming from the muon decay. The result is $P_\mu = -0.790 \pm 0.025$ at 190 GeV beam energy. The target, subdivided into two cells polarised in opposite directions, was typically polarised up to 50% for the deuteron and 85% for the proton target. The target spin directions were reversed 5 times a day. Polarisation of the SLAC electron beam reached 86% in the E143 and was randomly reversed. Polarisation of the targets reached 80% for the proton and 25% for the deuteron one in E143. Systematic uncertainties in the SMC and SLAC experiments are similar.

4.3. Results of the measurements and spin structure of the nucleon

Cross section asymmetries A_1 and spin dependent structure functions g_1 have been measured for the proton and deuteron targets by the SMC, [63–66] and by the E143, [68, 69]. Information on the neutron has been evaluated from the data on ^{3}He (E142, [67]) and from the data on the proton and deuteron (SMC, [63, 64]). All data sets are in a very good mutual agreement even if A_1, extracted from data covering different Q^2 intervals, has been assumed to be Q^2 independent.

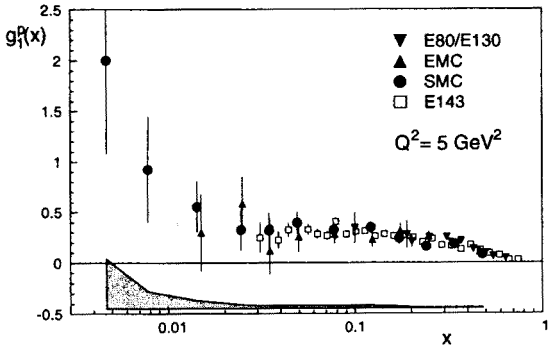

Fig. 4.1. The spin dependent structure function $g_1(x)$ of the proton at Q^2=5 GeV^2. the EMC data were reevaluated using the same F_2 and R parametrisations as for the SMC and E143 data. Error bars are statistical; the shaded area marks the SMC systematic errors. Figure taken from [62].

Results on g_1 for proton, deuteron and neutron are shown in Figs. 4.1 and 4.2. Here $g_1^n = 2g_1^d/(1 - 1.5\omega_D) - g_1^p$ where $\omega_D \sim 0.05$ is the probability of the D-state of the deuteron. Conversion of A_1 to g_1, which was

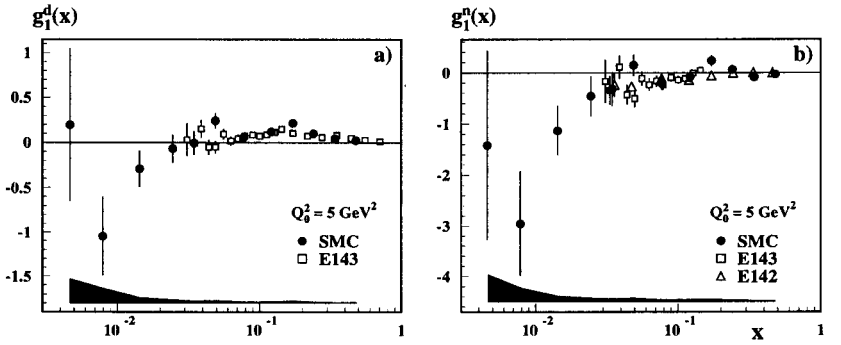

Fig. 4.2. The spin dependent structure functions (a) $g_1^d(x)$ and (b) $g_1^n(x)$, as a function of x at Q_0^2=5 GeV^2. Error bars are statistical; the shaded area marks the SMC systematic errors. Figure taken from [64].

made under an assumption that A_1 scales, needs only information on the structure function F_1 or, equivalently, F_2 and R (*cf.* Eq. (4.6)). The NMC parametrisation of $F_2(x, Q^2)$ [49] and the SLAC parametrisation of $R(x, Q^2)$ [32] have been used by both SMC and SLAC. The behaviour of the g_1^p is different from that of g_1^d and g_1^n, especially at low x. This should be contrasted with the unpolarised case where a small difference between proton and neutron structure functions can be explained by nuclear shadowing in the deuteron. Measurements of the asymmetry, A_2, for the proton [66] and the deuteron [70] showed that this function is significantly smaller than the bound $\sqrt{R}$ and consistent with zero.

The Bjorken sum rule seems to be fulfilled by the above data at the 10% level: its value measured by the SMC at Q^2 =10 GeV^2 is $\Gamma_1^p - \Gamma_1^n$ =0.199±0.038, to be compared with the QCD prediction (four flavours, corrections up to α_S^3): 0.187±0.003. The Ellis–Jaffe sum rule is not confirmed by the data, the pattern of disagreement being similar in the proton and deuteron results. At Q^2 = 5 GeV^2, the combined data of the EMC, SMC and SLAC give for Γ_1^p, Γ_1^d and Γ_1^n respectively: 0.125±0.009, 0.041±0.005 and −0.037±0.008 as compared to the predicted 0.167±0.005, 0.070±0.004 and −0.015±0.005. A most straightforward explanation of this violation may be a non–zero polarisation of the strange sea. Results of the new SMC proton data analysis, with extended kinematic coverage and a NLO QCD analysis to evolve the measured $g_1(x, Q^2)$ to a common value of Q^2, confirm all the above conclusions.

The nucleon spin, $S_z = \frac{1}{2}$, can be decomposed as follows

$$S_z = \tfrac{1}{2}\Delta\Sigma + \Delta g + L_z\,, \tag{4.10}$$

where L_z is angular momentum due to the partons. All the data sets (except perhaps E142), evaluated with a consistent treatment of the QCD corrections at a common Q^2=5 GeV^2 and under the assumption that the flavour SU(3) is exact, show that the total quark contribution to the nucleon spin is small, $\Delta\Sigma \sim 0.2$, and that the strange sea is indeed polarised: $\Delta s \sim -0.1$. SU(3)–breaking can decrease Δs but leaves $\Delta\Sigma$ unchanged. Choosing a factorization scheme in which the quarks polarisation is scale independent, a Q^2 dependent gluonic contribution appears in the Ellis–Jaffe sum rule as a result of the anomalous dimension of the singlet axial vector current [61]. Then the Ellis–Jaffe assumption of Δs=0 implies that at Q^2=5 GeV^2, $\Delta g \sim 3$ is needed to restore the sum rule.

Finally we note the first measurements of the semi–inclusive spin asymmetries for positively and negatively charged hadrons in the polarised muon–proton and muon–deuteron scattering in the SMC experiment [71]. The x dependence of the spin distributions for the up and down valence quarks and for the non-strange sea quarks has been determined. The moments of the quark spin distributions were obtained to be: Δu_v=1.01$\pm$0.24, Δd_v = -0.57 ± 0.25; moments for the non-strange sea quarks are consistent with zero over the whole measured range of x.

4.4. Prospects for the future

Understanding of the polarised structure functions has improved dramatically in the recent years, thanks to the EMC, SMC and SLAC measuremets. Several questions however remained unanswered. Among them is the low x behaviour of g_1, its Q^2 evolution, the gluon polarisation and flavour decomposition of polarised parton distribution. The HERMES experiment, recently starting at HERA, using a polarised electron beam and a polarised internal gas target will especially address the last question from a presently unique reconstruction of the hadronic final state. To answer the remaining questions a new generation of experiments, *e.g.*at the HERA *collider*, is needed. Prospects of spin physics at HERA were discussed at a workshop at DESY–Zeuthen in August 1995. A polarised deep inelastic programme at HERA could allow measurements over an extended kinematic range, including low x and high Q^2. Polarisation of the proton beam is technically much more complicated than polarisation of the electron beam, as the proton beam does not polarise naturally [72]. Construction of the polarised proton beams of energy up to 250 GeV in the RHIC collider rings has already been approved, a helpful step for HERA. Various suggestions

for dedicated measurements of $\Delta g(x,Q^2)$, including the HMC/CHEOPS project at CERN, were also discussed at the Zeuthen workshop [73].

5. Conclusions

This review, together with a similar one by A. De Roeck in these proceedings and devoted to HERA results, [11] gives a summary of data on the structure of the (free and bound) nucleon as it is seen in deep-inelastic lepton scattering. The (non-polarised) fixed-target experimental programme comes soon to an end thus closing an epoque in the high energy physics. Sound and spectacular knowledge has been obtained as a result of a great effort of many experiments. In particular convincing QCD tests were performed, the parton distributions at $x \gtrsim 0.01$ were well determined (except possibly these for gluons) and nuclear effects in deep inelastic scattering, especially at low x were well measured.

At the end of the fixed-target deep inelastic programme complementary measurements of HERA started to deliver results. The HERA data join well the fixed-target ones. In spite of a (still) much lower level of accuracy of the former, a joint QCD analysis is already possible in a large kinematic interval. In a physics picture which emerges from all the data the most puzzling phenomenon is the rise of F_2 at small x, apparently persisting even at moderate values of Q^2 ($Q^2 \sim 1.5$ GeV^2) as well as its connection with the soft Pomeron seen in photoproduction at $Q^2 = 0$.

Spin structure of the nucleon also seems to be puzzling in the small-x region, somewhat analogous to the unpolarized case. Namely, the lowest-x data points for the proton spin structure functions g_1 indicate the possibility of a rise at small x. At the same time QCD calculations predict at strong rise of g_1 at small x. Naturally for the fixed-target data, the non-perturbative effects interfere with the low x dynamics. So there is little doubt that small x, small Q^2 physics is becoming a field of particular interest.

My thanks to the organizers for the splendid conference, to my colleagues from the NMC and SMC and to Jan Kwieciński for the most enjoyable research collaboration. A large portion of this article I have written as a part of the Working Group Report on the Structure of the Proton which summarizes activities of the Group during the Workshop on "HERA Physics: Proton, Photon and Pomeron Structure", held in Durham, in September 1995. I am grateful to A.D. Martin, A. De Roeck and T. Gehrmann for the fruitful and inspiring collaboration in writing the Report. My attendance at the conference was partially supported by the Polish State Committee for Scientific Research grant number 2 P302 062 04.

REFERENCES

[1] Working Group Report on the *Structure of the Proton*, to be published in the Proceedings of Durham 1995 Workshop on "HERA Physics: Proton, Photon and Pomeron Structure", *J. Phys. G.*

[2] NMC: M. Arneodo *et al. Phys. Lett.* **B364**, 107 (1995).

[3] L.W. Whitlow *et al. Phys. Lett.* **B282**, 475 (1992).

[4] BCDMS Collaboration: A. C. Benvenuti *et al. Phys. Lett.* **B223**, 485 (1989) 485; *ibid* **B237**, 592 (1990).

[5] EMC NA28: M. Arneodo *et al. Nucl. Phys.* **B333**, 1 (1990).

[6] J. Kwieciński, B. Badełek, *Z. Phys.* **C43**, 251 (1989); B. Badełek, J. Kwieciński, *Phys. Lett.* **B295**, 263 (1992).

[7] E665 Collaboration: A. V. Kotwal *et al.* preprint FERMILAB-CONF-95-46 and to appear in Proc. of the XXX Rencontre de Moriond, *QCD and High Energy Hadronic Interactions*, March 1995, Les Arcs, France; A.V. Kotwal, Ph.D. Thesis, Harvard University, May 1995.

[8] F. Eisele, to appear in Proc. of Int. Europhysics Conference on High Energy Physics, Brussels, 1995 and DESY preprint 95-229.

[9] A. Levy, to be published in the Proceedings of Durham 1995 Workshop on "HERA Physics: Proton, Photon and Pomeron Structure", *J. Phys. G.*

[10] A.D. Martin, W.J. Stirling, R.G. Roberts, *Phys. Lett.* **B306**, 145 (1993) 145; A.D. Martin, W.J. Stirling, R.G. Roberts, *Phys. Rev.* **D47**, 867 (1993).

[11] HERA, H1 Collaboration, A. De Roeck, these proceedings.

[12] NMC: A. Dyring, Proc. of the XXIX Rencontre de Moriond, *QCD and High Energy Hadronic Interactions*, March 1994, Méribel, France, edited by J. Trân Thanh Vân, Editions Frontières.

[13] NMC: M. Arneodo *et al. Phys. Rev.* **D50**, R1 (1994).

[14] E665 Collaboration: M.R. Adams *et al. Phys. Lett.* **B309**, 477 (1993).

[15] E665 Collaboration: M.R. Adams *et al. Phys. Rev. Lett.* **75**, 1466 (1995).

[16] B. Badełek, J. Kwieciński, *Phys. Rev.* **D50**, R4 (1994).

[17] W. Melnitchouk, A.W. Thomas, *Phys. Rev.* **D47**, 3783 (1993); *Phys. Lett.* **B317**, 437 (1993); V. Barone *et al. Phys. Lett.* **B321**, 137 (1994).

[18] V.R. Zoller, *Phys. Lett.* **B279**, 145 (1992); *Z. Phys.* **C54**, 425 (1992).

[19] NMC: A. Witzmann, Proc. of Int. Europhysics Conf. on High Energy Physics, Brussels 1995.

[20] NMC: P. Amaudruz *et al. Nucl. Phys.* B441, 3 (1995).

[21] NMC: P. Amaudruz *et al. Nucl. Phys.* B441, 12 (1995).

[22] E139 Collaboration: R.G. Arnold *et al. Phys. Rev. Lett.* **52**, 727 (1984).

[23] E665 Collaboration: M.R. Adams *et al. Z. Phys.* **C67**, 403 (1995).

[24] NMC: A. Mücklich, Proc. of the Workshop on the Deep Inelastic Scattering and QCD, Paris, 1995, eds J.-F. Laporte and Y. Sirois, p. 489.

[25] E665 Collaboration: T. Carroll, to be published in the Proceedings of Durham 1995 Workshop on "HERA Physics: Proton, Photon and Pomeron Structure", *J. Phys. G.*

[26] NMC: M. Arneodo *et al. Phys. Lett.* **B309**, 222 (1993).

[27] M. Virchaux and A. Milsztajn, *Phys. Lett.* **B274**, 221 (1992).
[28] NMC: P. Amaudruz *et al. Phys. Lett.* **B294**, 120 (1992).
[29] NMC: T. Granier, Proc. of the XXIX Rencontre de Moriond, *QCD and High Energy Hadronic Interactions*, March 1994, Méribel, France, edited by J. Trân Thanh Vân, Editions Frontières.
[30] NMC: A. Dyring, PhD, Uppsala University (1995).
[31] CCFR Collaboration: U.K. Yang, to be published in the Proceedings of Durham 1995 Workshop on "HERA Physics: Proton, Photon and Pomeron Structure", *J. Phys. G.*
[32] L.W. Whitlow *et al. Phys. Lett.* **B250**, 193 (1990).
[33] B. Badełek, J. Kwieciński, A. Staśto, Durham preprint DTP/96/16.
[34] S.A. Larin and J.A.M. Vermaseren, *Phys. Lett.* **B259**, 345 (1991).
[35] CCFR Collaboration: D.A. Harris *et al.* to appear in the Proc. of Int. Europhysics Conf. on High Energy Physics, Brussels 1995. EPS-0043.
[36] NA51 Collaboration: A. Baldit *et al. Phys. Lett.* **B332**, 244 (1994).
[37] NMC: A. Brüll, Proc. of Int. Europhysics Conf. on High Energy Physics, Brussels 1995.
[38] B. Badełek, J. Kwieciński, to appear in the April 1996 issue of *Rev. Mod. Phys.*
[39] B. Badełek *et al. Rev. Mod. Phys.* **64**, 927 (1992).
[40] F.W. Brasse *et al. Nucl. Phys.* **B110**, 413 (1976).
[41] CHIO Collaboration: Gordon *et al. Phys. Rev.* **D20**, 2645 (1979).
[42] A. Donnachie, P.V. Landshoff, *Z. Phys.* **C61**, 139 (1994).
[43] H. Abramowicz *et al. Phys. Lett.* **B269**, 465 (1991).
[44] NMC: P. Amaudruz *et al. Nucl. Phys.* **B371**, 3 (1992).
[45] A. Capella *et al. Phys. Lett.* **B337**, 358 (1994).
[46] M. Glück, E. Reya, A. Vogt, *Z. Phys.* **C67**, 433 (1995).
[47] G.A. Schuler, T. Sjöstrand, *Nucl. Phys.* **B407**, 425 (1993).
[48] A.D. Martin, W.J. Stirling, R.G. Roberts, *Phys. Rev.* **D51**, 4756 (1995).
[49] NMC: P. Amaudruz *et al. Phys. Lett.* **B295**, 159 (1992 and preprint CERN-PPE/92-124; Erratum Oct. 26th, 1992; Erratum April 19th, 1993.
[50] E665 Collaboration: M.R. Adams *et al. Phys. Rev. Lett.* **68**, 3266 (1992).
[51] J. Kwieciński, to be published in the Proceedings of Durham 1995 Workshop on "HERA Physics: Proton, Photon and Pomeron Structure", *J. Phys. G.*
[52] R.L. Jaffe, *Comm. Nucl. Phys.* **19**, 239 (1990).
[53] R. Mertig, W.L. van Neerven, Leiden preprint INLO-PUB-6/95 (revised); W. Vogelsang, Rutherford Laboratory preprint RAL-TR-95-071.
[54] T. Gehrmann, W.J. Stirling, Proc. of the Workshop on the Prospects of Spin Physics at HERA, Zeuthen, August 1995, eds J. Blümlein and W.-D. Nowak (1995), p.295.
[55] J.D. Bjorken, *Phys. Rev.* **148**, 1467 (1966); *ibid.* **D1**, 465 (1970); *ibid.* **D1**, 1376 (1970).
[56] S.A. Larin, F.V. Tkachev, J.A.M. Vermaseren, *Phys. Rev. Lett.* **66**, 862 (1991); S.A. Larin, J.A.M. Vermaseren, *Phys. Lett.* **B259**, 345 (1991).
[57] A.L. Kataev, V. Starchenko, CERN-TH-7198/94.

[58] J. Ellis, R.L. Jaffe, *Phys. Rev.* **D9**, 1444 (1974); Erratum *ibid.* **D10**, 1669 (1974).
[59] S.A. Larin, *Phys. Lett.* **B334**, 192 (1994).
[60] A.L. Kataev, *Phys. Rev.* **D50**, 5469 (1994).
[61] C.S. Lam, Bing-An Li, *Phys. Rev.* **D25**, 683 (1982).
[62] R. Voss, Proc. of the Workshop on the Deep Inelastic Scattering and QCD, Paris, April 1995, eds J.-F. Laporte and Y. Sirois, p.77.
[63] SMC: B. Adeva *et al. Phys. Lett.* **B302**, 533 (1993).
[64] SMC: D. Adams *et al. Phys. Lett.* **B357**, 248 (1995).
[65] SMC: D. Adams *et al. Phys. Lett.* **B329**, 399 (1994); Erratum, *Phys. Lett.* **B339**, 332 (1994).
[66] SMC: B. Adeva *et al. Phys. Lett.* **B336**, 125 (1994).
[67] E142 Collaboration: P.L. Anthony *et al. Phys. Rev. Lett.* **71**, 959 (1993).
[68] E143 Collaboration: K. Abe *et al. Phys. Rev. Lett.* **74**, 346 (1995).
[69] E143 Collaboration: K. Abe *et al. Phys. Rev. Lett.* **75**, 25 (1995).
[70] E143 Collaboration: K. Abe *et al. Phys. Rev. Lett.* **76**, 587 (1996).
[71] SMC: B. Adeva *et al.* CERN-PPE/95-187 and *Phys. Lett.* (in print).
[72] Proc. of the Workshop on the Prospects of Spin Physics at HERA, Zeuthen, August 1995, eds J. Blümlein and W.-D. Nowak (1995), p. 76-99.
[73] Proc. of the Workshop on the Prospects of Spin Physics at HERA, Zeuthen, August 1995, eds J. Blümlein and W.-D. Nowak (1995), p. 248–282.